JOURNAL OF CATALYSIS 139, 191–206 (1993)

Supported Metal Catalysts: Preparation, Characterisation, and Function

I. Preparation and Physical Characterisation of Platinum Catalysts

S. D. JACKSON,*,[1] J. WILLIS,* G. D. MCLELLAN,† G. WEBB,†,[1] M. B. T. KEEGAN,‡ R. B. MOYES,‡ S. SIMPSON,‡ P. B. WELLS‡,[1], AND R. WHYMAN§,[1]

*ICI Katalco, Research and Technology Group, P.O. Box 1, Billingham, Cleveland TS23 1LB, United Kingdom; †Department of Chemistry, The University, Glasgow G12 8QQ, Scotland; ‡School of Chemistry, The University, Hull HU6 7RX, United Kingdom; and §ICI Chemicals and Polymers, Ltd., Research and Technology Department, P.O. Box 11, The Heath, Runcorn, Cheshire WA7 4QE, United Kingdom

Received June 7, 1991; revised May 8, 1992

The preparation, by impregnation (I), co-crystallization (C), and metal vapour deposition (M), of a range of silica-, alumina-, and molybdena-supported platinum catalysts is described. These materials (and the supports) have been thoroughly characterised in both pre- and postreduction states using a wide range of physical techniques including electronic spectroscopy, TGA, TPR, XPS, HRTEM, and EXAFS. UV–visible spectroscopic data for the impregnated materials is consistent with the presence of octahedral Pt(IV) environments in the prereduction state. Pt/silica (I) is essentially chloride-free after reduction, whereas Pt/alumina (I) retains a significant amount of chloride which is associated with the support rather than the metal. Pt/silica (M) is chloride-free and Pt/alumina (M) contains no more than the residual chloride initially associated with the alumina support. TGA and TPR data are largely as expected and, in the case of the molybdena-supported catalysts, are consistent with hydrogen bronze formation upon reduction. XPS data are consistent with the presence of Pt(0) in Pt/alumina (M) and the reduction of platinum to the metallic state in the case of Pt/silica (I). In contrast, with Pt/alumina (I), Pt/molybdena (I), and Pt/molybdena (C), the metal retains a significant $\delta+$ character in the postreduction state. In the case of Pt/alumina (I), this behaviour is best interpreted in terms of a metal–support interaction, whereas that observed with the molybdena supports is consistent with hydrogen bronze formation. XPS, TGA, and TPR data show a high degree of internal consistency with respect to bronze stoichiometries. HRTEM and EXAFS data are self-consistent and, with the exception of Pt/molybdena (I), the platinum crystallites are extremely highly dispersed, with size distributions in the order Pt/alumina (M) ~ Pt/silica (M) < Pt/molybdena (C) < Pt/alumina (I) < Pt/silica (I) ≪ Pt /molybdena (I). Models for the platinum sites in Pt/alumina (I) and Pt/silica (I) have been developed.

INTRODUCTION

The central objective of this collaborative investigation has been to establish a framework of theory and practice within which the performance (i.e., activity, selectivity, and lifetime characteristics) of supported metal catalysts (particularly those containing Pt and Ni) can be evaluated and correlated with (i) the different preparative procedures used, (ii) the physical properties, and (iii) the chemical properties, both of the precursors and of the activated materials. The ultimate objective is to develop the capability of utilising this knowledge and understanding in a predictive capacity.

The following strategy has been adopted. Series of supported metal catalysts have been prepared using two traditional methods and one novel route, respectively, impregnation, co-crystallization, and metal vapour deposition. The supports which have been used include two traditional and one

[1] To whom correspondence should be addressed.

0021-9517/93 $5.00

less conventional one, namely, silica, alumina, and molybdena. The supports have been fully characterised and stages in the preparative procedures carefully controlled and monitored.

The physical states of the active catalysts and their precursors have been characterised by high-resolution transmission electron microscopy (HRTEM), X-ray photoelectron spectroscopy (XPS), secondary ion mass spectrometry (SIMS), X-ray diffraction (XRD), extended X-ray absorption fine structure (EXAFS), thermogravimetric analysis (TGA), temperature-programmed reduction (TPR), FTIR spectroscopy, UV–visible spectroscopy, and microanalysis. The chemical states of the active catalysts have been characterised by pulse and static chemisorption measurements and *in situ* FTIR spectroscopy incorporating isotope tracer techniques (both stable and radioactive tracers). The use of tracer techniques has played an important role in attempts to delineate the character and role of the adsorbed hydrocarbonaceous species. Adsorbates employed have included carbon monoxide, carbon dioxide, dioxygen, dihydrogen, ethene, and ethyne. Ethene adsorption has been studied both alone and competitively in the presence of carbon monoxide. Combinations of these techniques have provided, as expected, estimates of site densities in the activated catalysts. In addition, in the case of platinum, they have revealed unusual behaviour in terms of (i) concentrations of reactive hydroxyl functionalities which participate in the water gas shift reaction, (ii) subsurface hydrogen which may be liberated or locked in depending upon the adsorbent, and (iii) a special form of adsorbed hydrogen associated with partially oxidised surfaces. The catalysts have been studied in respect of a wide variety of reactions ranging from mild hydrogenations of diagnostic significance to demanding reactions of industrial importance. These have included the hydrogenations of carbon monoxide, buta-1,3-diene, and cyclopropane, and the hydrogenolyses of *n*-butane and propane.

A large amount of analytical and characterisation work has been undertaken in support of this project and, in addition to the principal investigators, a total of approximately 25 staff have contributed to various aspects of the work at the four centres. Characterisation methods such as TPR, FTIR, and gas chemisorption are available at each centre, and duplicate determinations have therefore been used as a check to ensure agreement and reproducibility of results between laboratories.

Throughout this paper and in subsequent publications a standard nomenclature has been adopted to designate the catalyst preparation method. Catalysts designated (I) have been prepared by impregnation, catalysts designated (C) have been prepared by co-crystallization, and catalysts designated (M) have been prepared by metal vapour deposition.

In the first series of papers we describe results obtained using the supported platinum catalysts. A similar series of papers will describe the results obtained from parallel studies of the supported nickel catalysts.

EXPERIMENTAL

Preparation of the Catalyst Precursors

Impregnation (I). A quantity of 9.76 g of hexachloroplatinic acid (Johnson Matthey, platinum assay 41.0%) was dissolved in deionised water (600 ml) in a 5-liter round-bottomed flask. Silica (M5 Cab-O-Sil) was added and mixed until the suspension began to gel, at which point further deionised water (ca 500 ml) was added to promote mobility. This process was repeated until all the silica (398.0g) had been introduced, the total volume of water required being 2.5 liter. The flask was attached to a Buchi rotary evaporator and the water slowly removed by maintaining the contents at 353 K under a partial pressure of dry dinitrogen. After 48 h a pale yellow free-flowing powder was obtained.

A similar procedure was adopted for the preparation of the alumina (Degussa Alu-

minium Oxid C) and molybdena (BDH Analar grade, 99.5%) supported catalysts.

Co-crystallization (C). Platinum molybdenum (VI) oxide was prepared by the co-crystallization of molybdenum (VI) trioxide and tetrammine platinum (II) chloride. A quantity of 497.8 g of molybdenum (VI) trioxide (Analar grade) was dissolved in concentrated aqueous ammonia solution (2.0 liter); complete dissolution was effected by warming the mixture on a hot water bath. Platinum (II) chloride (3.67 g) (Johnson Matthey Chemicals Ltd) in deionised water (80 ml), with pH 2.6, was added, resulting in a solution of pH 9.4. Neutralisation with concentrated hydrochloric acid (100 ml) produced a solution of pH 7.7 and a precipitate of molybdenum (VI) trioxide. The precipitate was redissolved by the addition of concentrated ammonia solution (65 ml) and some gentle warming. The co-crystallized product was then formed by the rotary evaporation of the final solution at 343 K over an extended period (about 2 days). The distillate had pH values ranging between 11.3 and 11.7.

Metal vapour deposition (M). The precursor complex, bis-toluene platinum, was prepared by metal vapour synthesis techniques using a commercial positive hearth electrostatically focussed electron beam rotary metal atom reactor (*1*). Platinum metal (0.70 g) was evaporated over 3 h and co-condensed at 77 K with degassed, sodium-dried toluene (ca 200 ml). After warm-up and melting, the dark brown toluene solution of $Pt(toluene)_2$ was transferred under anaerobic conditions at 213 K from the reactor flask into a Schlenk receiver vessel. Aliquots of this solution, filtered through celite at 195 K, were added to dry toluene suspensions of silica (15.0 g) or alumina (15.0 g) also maintained at 195 K. The support materials were previously dried overnight at 773 K under a flow of dry dinitrogen. The mixtures were stirred for 3 h at 195 K and then slowly allowed to warm to room temperature under dinitrogen. Excess toluene was removed under flowing dinitrogen and cold-trapping, and after 2 days the products were transferred to a glove box as homogeneous, air-sensitive, light brown free-flowing powders.

Standard Reduction Procedure

The following standard reduction procedure was adopted for the impregnated and co-crystallized catalyst precursors, using a standard catalyst weight of 0.25 ± 0.05 g:

(i) 30 min at ambient temperature in flowing 6% H_2/N_2;

(ii) heat to 573 K in flowing H_2/N_2 (25 ml/min) and monitor the eluent;

(iii) leave for 30 min at 573 K after the trace returns to the baseline;

(iv) purge with helium at 573 K until no H_2 is detected in the eluent;

(v) cool in flowing helium to the required temperature; and

(vi) store the sample in static dioxygen-free helium.

Methods of Characterisation

Elemental analysis. Elemental analyses were carried out by inductively coupled plasma—mass spectrometry (ICP-MS). In addition chloride levels were determined by chemical analysis coupled with X-ray fluorescence (XRF).

Surface area measurements. Determination of surface areas of the catalyst supports, both before and after treatment with water (in order to simulate the impregnation procedure), and of Pt/silica (I) and Pt/alumina (I), was carried out using standard N_2 BET methods; full isotherms were measured. In addition the silica N_2 isotherm was analysed using the Alpha-s method (*2*) and good agreement with the BET plot was demonstrated.

Ultraviolet–visible spectroscopy. Ultraviolet–visible spectra of the solid catalyst precursors were recorded over the range 190–800 nm using a Philips 8800 UV–visible spectrometer with a diffuse reflectance attachment. Spectra of solutions were recorded using standard 1-cm cells.

Thermogravimetric analysis (TGA). Thermogravimetric analyses were carried out using a Du Pont Model 1090 thermograv-

imetric analyser and a heating rate of 10 K min^{-1} either in flowing dinitrogen or flowing 5% H_2/N_2.

Temperature-programmed reduction (TPR). The temperature programmed reduction studies were performed using a pulse-flow microreactor system. Using this system the catalysts could be reduced *in situ* in flowing 5% H_2/N_2 by heating to 573 K. After reduction had ceased the flow was changed to helium and catalyst held at 573 K until no dihydrogen could be detected in the reactor effluent. The catalyst was cooled and maintained in flowing helium. The temperature programmed reductions were followed using a TCD gas chromatograph coupled to a mass spectrometer (Spectramass SM1000D, fitted with a high-resolution RF head).

X-ray photoelectron spectroscopy (XPS). Spectra were collected using either a Kratos XSAM 800 electron spectrometer or a VG ESCALAB-200D instrument. The pressure was maintained at $\simeq 10^{-9}$ mbar during analyses. Air-sensitive samples were handled in a glove box and transferred to the spectrometer under dinitrogen. The Pt(4*f*), Pt(4*d*), Mo(3*d*), Al(2*p*), Si(2*p*), O(1*s*), Cl(2*p*), and C(1*s*) photolines were monitored, where appropriate. Spectra were initially calibrated with reference to the C(1*s*) line (285.0 eV) and platinum binding energies normalised against the Si(2*p*) (104.1 eV), Al(2*p*) (74.6 eV), and Mo(3*d*) (233.3 eV) values of the respective supports. A number of reference samples were also analysed to provide the background information necessary for the interpretation of the spectra of the catalysts.

X-ray diffraction (XRD). X-ray diffraction measurements were carried out on a Siemens automatic powder diffraction system which incorporated in-situ reduction facilities. Cu $K\alpha$ radiation was used.

Secondary ion mass spectrometry (SIMS). SIMS spectra of the samples were recorded using an I.S.A. Riber instrument (Rueil–Malmaison, France). The powder samples were pressed into discs for the measurements.

High-resolution transmission electron microscopy (HRTEM). High-resolution transmission electron microscopy was carried out using a Jeol 200C instrument. Specimens were examined by two methods, namely, (i) dispersion in *n*-hexane and evaporation onto copper grids coated with thin carbon films and (ii) after sectioning from Araldite. Magnifications ranging between 90,000 and 450,000 were used. For each micrograph in excess of 250 particles were sized unless, as with one of the Pt/silica samples, significant beam damage was apparent.

Extended X-ray absorption fine structure spectroscopy (EXAFS). Transmission EXAFS spectra of samples at the Pt L_3-edge were collected at the Synchrotron Radiation Source at the SERC Daresbury Laboratory. Powdered samples were reduced at 573 K and examined under pure dihydrogen at ambient temperature in specially constructed glass cells fitted with Mylar windows. The spectra were analysed using Curved Wave Theory. Phase-shift files as calculated by EXCURV90 were refined using Pt foil as a model. The phase shifts thus arrived at were used for the supported catalysts. Multiple scattering effects were not included.

RESULTS AND DISCUSSION

Characterisation of Support Materials

The supports have been fully characterised in respect of (i) their surface area and pore volume; (ii) their full analysis by ICP-MS, chemical analysis, XRF and XPS; and (iii) their stability and behaviour during TGA. The measured surface areas and impurity levels are summarised in Table 1. From these data it is clear that the chloride level in alumina comprises the only significant impurity of potential catalytic significance. The surface areas recorded in Table 1 were, within experimental error, unchanged following impregnation, reduction, and reoxidation.

TABLE 1

Properties of Support Materials

	Surface area (m^2g^{-1})	Impurities (ppm)
SiO_2 (M5 Cab-O-Sil)	203	Cl(537), Cu(20), Na(20)
Al_2O_3 (Degussa Aluminium Oxid C)	102	Cl(2780), Fe(110), Zn(90), Ni(45), other elements below 35
MoO_3 (BDH Analar, 99.5%)	2.1	Cl(0), Pb(1000 max), Fe(500 max), Cu(500 max)

Note. All samples have zero pore volume.

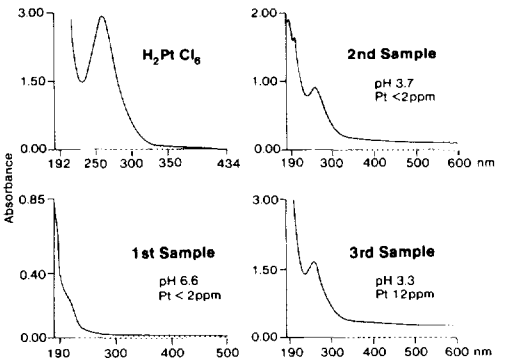

FIG. 1. Ultraviolet–visible solution spectra of aqueous H_2PtCl_6 and of liquor collected at successive stages during the drying process in the preparation of Pt/silica (I).

Characterisation of Supported Materials during Preparation and before/after Reduction

The impregnated and co-crystallized catalyst precursors were prepared under carefully controlled conditions and stages in the preparation procedure monitored using UV–visible spectroscopy and pH measurements. The appearance of a coloured distillate in the collection flask during the removal of water from the H_2PtCl_6/silica preparation suggested the volatilisation of hexachloroplatinic acid. Representative UV–visible solution spectra of aqueous H_2PtCl_6 and of liquor collected at successive stages during the drying process, together with pH data, are shown in Fig. 1. These data are consistent with the presence of hexachloroplatinic acid in the distillates. As expected, the pH values decrease as the platinum concentration increases. As a consequence of this behaviour the platinum content of the dried, supported material was significantly less than the expected 1 wt% based on the quantities of reagent used. This steam distillation of H_2PtCl_6 was not apparent during the preparation of the impregnated alumina and molybdena samples. Characterisation of the dried, supported materials prior to reduction was effected by a combination of UV–visible spectroscopy, microanalysis, and XPS. Stages in the processes occurring during thermal treatment and reduction were monitored by TGA and TPR. Characterisation of the reduced and used catalysts was carried out using a combination of microanalysis, XPS, TEM, EXAFS, XRD, and SIMS. The collective data which have been obtained are summarised under the appropriate technique heading.

Ultraviolet–visible spectra. The absorption maxima and band assignments of the UV–visible spectra of the dried, supported materials prepared by aqueous impregnation are recorded in Table 2, together with data for aqueous hexachloroplatinic acid for the purposes of comparison. The UV–visible spectroscopic data on the impregnated

TABLE 2

Absorption Maxima (nm) and Band Assignments of UV–Visible Spectra of Catalysts Prepared by Aqueous Impregnation

	Transition		LMCT[a]
	$^1A_{1g} \rightarrow {}^1T_{2g}$	$^1A_{1g} \rightarrow {}^1T_{1g}$	
Pt/SiO_2(I)	456	374	264 206
Pt/Al_2O_3(I)	452	354	218
Pt/MoO_3(I)	450[b]		
PtO_2/Al_2O_3	450	359	209
$[PtCl_6]^{2-}$ aqueous	452	362	263 205

[a] LMCT: ligand-to-metal charge transfer.
[b] Remainder of spectrum obscured by MoO_3.

materials compares well with the available literature data on octahedral platinum (IV) species (*3, 4*). In particular, the spectrum of Pt/silica (I) in the prereduction state is very similar to that of H_2PtCl_6 in aqueous solution. The spectrum of the Pt/alumina (I) sample is slightly different, as evidenced by the shift of the ligand-to-metal charge-transfer (LMCT) transition to 218 nm. This spectrum is in fact similar (see Table 2) to that displayed by an authentic sample of PtO_2/alumina (I), in which the 209-nm absorption is assigned to LMCT from O to Pt. The presence of an intermediate hydroxy- or oxychloro species such as $[PtCl_5OH]^{2-}$, formed by exchange reactions of the type

$$[PtCl_6]^{2-} + H_2O \rightleftharpoons [PtCl_5OH]^{2-} + H^+ + Cl^-$$

in aqueous solution could therefore account for the observation of the 218-nm band in the spectrum of Pt/alumina (I). The spectra of these samples are invariant with respect to time, no differences being noted after 3 years storage.

In the light of the apparent discrepancy between the UV–visible spectra and the XPS data, discussed below, it should be emphasised that there is no obvious evidence from electronic spectroscopy for the presence in the bulk, as distinct from the surface as probed by XPS, of Pt(II) species. The spectra of the latter, assuming a square planar geometry, would be expected to display significantly different absorption band patterns of lower intensity than the equivalent octahedral Pt(IV) species. For example, aqueous solutions of $PtCl_2$ display weak absorptions at 437, 369, and 305 nm which correspond closely with the known spectrum of *trans*-$PtCl_2(H_2O)_2$ (*5*).

Microanalysis. Microanalytical data for platinum and chloride, together with the chloride content of the support materials, for the catalysts in their pre- and postreduction states, together with some used catalysts, are summarised in Table 3. From these data the following points are apparent. First, in the case of the catalysts prepared by aqueous impregnation and co-crystallization, the platinum content is essentially retained during the reduction procedure. Second, the Degussa alumina support material contains a significant concentration of chloride. Third, Pt/silica (I) and Pt/alumina (I) in their prereduction states have Cl/Pt ratios of approximately 5 and 6, respectively, after making allowance for the additional chloride present in the alumina support itself. These ratios are slightly at variance with the interpretation of the UV–visible spectra of these materials. Nevertheless, the data are consistent with the presence of higher, e.g. Pt(IV), rather than lower, e.g., Pt(II), oxidation states prior to reduction. Finally, Pt/alumina (I) retains most of the chloride initially present, both after reduction and also after subsequent exposure to carbon monoxide.

TABLE 3

Microanalytical Data

Method of preparation	Supports					
	SiO_2		Al_2O_3		MoO_3	
	A	B	A	B	A	B
	Platinum content (wt%)					
Impregnation	0.73	0.76	0.90	0.88	0.46	0.49
Co-crystallization	—	—	—	—	0.49	0.55
Metal vapour deposition	0.29		0.68		—	—
	Chloride content (wt%)					
	<0.02		0.27		<0.02	
Impregnation	0.64	<0.02	1.28	1.01 1.01[a] 1.00[b]	[c]	<0.02
Co-crystallization	—	—	—	—	<0.02	<0.02
Metal vapour deposition	<0.02		0.27		—	—

Note. Figures quoted to an accuracy of ±0.02. (A) Prereduction; (B) postreduction and storage in air.

[a] Post-reduction and storage under vacuum.

[b] Post-reduction and exposure to 7 × 50 μl CO.

[c] Detected but quantification impossible because of interference with Mo.

Thermogravimetric analysis (TGA). The impregnated and co-crystallized catalysts and the molybdena support were each examined by thermogravimetric analysis in both flowing dinitrogen and 5% H_2/N_2. The principal features of the TGA data for the

catalysts prepared by aqueous routes were largely as expected, namely, (i) a gradual loss of water under a dinitrogen flow and (ii) an additional feature in the presence of dihydrogen corresponding to the reduction of platinum. For example, Pt/alumina (I), on heating in dinitrogen, showed a continuous weight loss due to loss of water from the surface. When 5% H_2/N_2 was used an extra feature at 498–508 K, corresponding to reduction of the hexachloroplatinic acid, was noted. The main feature of the silica-supported sample when heated in dinitrogen was again a loss of water, although less than observed in the case of alumina. Under 5% H_2/N_2 there was a weight loss feature at 393–473 K which appeared to be made up of two components. This is in good agreement with results from the TPR experiment which gave a peak at 405 K, asymmetric to the high-temperature side. On heating molybdena in dinitrogen or 5% H_2/N_2 no weight loss was observed until 973 and 923 K, respectively, at which point a catastrophic change, due to sublimation of the oxide, was noted. When Pt/molybdena (I) was heated in dinitrogen a series of stepped weight losses was observed, up to a temperature of 773 K. This behaviour may be explained in terms of stepwise losses of HCl, H_2O, and O_2 from $H_2PtCl_6 \cdot 6H_2O$ during decomposition and formation of Pt/molybdena, viz.,

$$H_2PtCl_6 \cdot 6H_2O \rightarrow Pt + 6HCl + 4H_2O + O_2.$$

On heating in 5% H_2/N_2 a highly unusual feature was observed, namely, a weight *gain* above 398 K. This phenomenon is due to the uptake of hydrogen by the sample during the formation of a hydrogen bronze. If no account is taken of any losses then the material formed would have an empirical formula $H_{0.9}MoO_3$. However, after allowing for some losses due to decomposition/reduction of the chloroplatinic acid (which must occur to some extent before bronze formation), the hydrogen content in the formula could increase to $H_{1.2}MoO_3$. This figure is in good agreement with those obtained from TPR and XPS (see later).

In the case of the $PtCl_2/MoO_3/NH_4Cl$ sample prepared by co-crystallization, TGA was initially used to establish the most appropriate temperature at which to fire/calcine the material prior to reduction and generation of Pt/molybdena (C). The extent of weight loss in air was found to be greatest in the temperature range 423–673 K and corresponds with the decomposition of ammonium chloride and/or ammonium paramolybdate. The bulk of the sample was therefore fired/calcined at 723 K, during which decomposition of the platinum oxide to platinum metal occurred, as observed with Pt/molybdena (I), and a further TGA was carried out on the resulting product. Under a flow of dinitrogen alone, as expected, no change was noted until the onset of sublimation of MoO_3 at ca. 1073 K. However, under a 5% H_2/N_2 flow a small weight increase was observed at ca. 370 K, corresponding with the formation of the hydrogen bronze. Once again, if no account is taken of any losses the bronze would have a stoichiometry $H_{0.5}MoO_3$. Subsequent weight losses observed at 500 and 570 K are consistent with loss of water and the formation of various bronze stoichiometries which are stable at different temperatures. The existence of a range of bronze stoichiometries is well established (*6*).

Temperature-programmed reduction (TPR). TPR measurements were carried out at three centres (Billingham, Glasgow, and Hull) and, although some differences of detail were noted, the results were in general agreement. Any discrepancies seem to be associated with different initial temperatures used in the measurements, e.g., 180 or 293 K.

All samples gave reduction peaks in the temperature range 300–500 K, summarised in Table 4, which could be assigned to the reduction of platinum to the metallic state. Additional maxima were observed at temperatures above 500 K. These appear to be associated with the reduction of the sup-

TABLE 4

TPR Data

Catalyst	Temperature (K) of reduction maxima	
Pt/SiO_2 (I)		400–410
Pt/Al_2O_3 (I)		500
Pt/MoO_3 (I)		405[a]
Pt/MoO_3 (C)	300	395[a]

[a] Includes bronze formation.

ports, for example, formation of molybdenum bronzes of differing stoichiometries (see TGA results).

Pt/alumina (I) gave a single reduction peak at 500 K at heating rates of both 10 K min^{-1} and 35 K min^{-1} in flowing 5% H_2/N_2. Pt/silica (I) gave a single reduction peak at 405 K when the heating rate was 10 K min^{-1}. However, this peak was asymmetric with a considerable tail on the high-temperature side of the maximum. When a heating rate of 35 K min^{-1} was used two peaks were observed, the first at 395 K and the second at 573 K, the ratio of peak areas being 2 : 1. The reduction profiles for the Pt/molybdena catalysts are complicated by the fact that the hydrogen bronze is produced, and although peak maxima are observed at 405 and 395 K, for the impregnated and co-crystallized catalysts, respectively, these maxima are not necessarily related simply to the reduction of the platinum. The latter event appears to commence at 338 K, a temperature at which a colour change is also noted. This is similar to the behaviour of the silica-supported sample. For Pt/molybdena (C) the area of the reduction peak at 303 K is in fact more than sufficient to account for the reduction of PtO_2 to platinum metal at this temperature.

An indication of the amount of reduction, as measured by hydrogen uptake, was obtained for each of the catalysts by measuring the peak areas as a function of platinum content. The H : Pt ratio per g-catalyst was 28 for Pt/silica (I), 23 for Pt/alumina (I), 323 for Pt/molybdena (I), and 259 for Pt/molybdena (C). Clearly the figures for the Pt/molybdena samples incorporate the hydrogen uptake associated with the formation of the hydrogen bronzes. If an H : Mo ratio is calculated, after allowing for the required 1 : 1 H : Cl ratio, values of 1.2 and 0.4 are obtained for Pt/molybdena (I) and Pt/molybdena (C), respectively.

TABLE 5

Surface Analytical Data for Supported Platinum Catalysts in the Pre- and Postreduction Stages

		Atom%						
		C(1*s*)	O(1*s*)	Pt(4*d*)	Cl(2*p*)	Si(2*p*)	Al(2*p*)	Mo(3*d*)
Pt/SiO_2(I)	A	6.1	62.7	<0.1	0.1	31.0	—	—
	B	6.5	62.6	<0.1	0.3	30.4	—	—
Pt/SiO_2(M)	A	4.8	63.8	<0.1	0.1	31.1	—	—
SiO_2		4.6	64.0	—	—	31.2	—	—
Pt/Al_2O_3(I)	A	9.9	53.6	0.2	1.3	—	34.9	—
	B	7.0	55.8	0.2	1.3	—	35.5	—
Pt/Al_2O_3(M)	A	9.8	54.2	<0.1	0.3	—	34.9	—
Al_2O_3		6.9	58.6	—	0.3	—	33.9	—
Pt/MoO_3(I)	A	26.0	47.4	1.5	5.7	—	—	19.3
	B	22.7	54.9	0.4	0.2	—	—	21.7
Pt/MoO_3(C)	A	33.9	46.6	0.2	—	—	—	18.2
	B	28.5	51.7	0.2	0.1	—	—	19.5
MoO_3		36.8	46.7	—	—	—	—	16.6

Note. (A) Prereduction; (B) postreduction.

These are in good agreement with the TGA results.

X-ray photoelectron spectroscopy (XPS). XPS data were recorded for all the supported platinum catalysts in both the pre- and postreduction states. In addition, representative samples were examined after reduction and storage in vacuo rather than in air. A number of reference samples were also analysed. The quantitative results of the analyses are summarised in Table 5, in which all elements detected are expressed as relative atomic percentages. The Pt(4*f*), Pt(4*d*), Mo(3*d*), Al(2*p*), Si(2*p*), O(1*s*), Cl(2*p*), and C(1*s*) photolines were monitored, where appropriate. In some cases coincidences in the signals caused difficulties in the interpretation of the spectra. For example, in the case of the alumina-supported samples, the strongest photoline of platinum, the Pt(4*f*) doublet, could not be detected because of its overlap with the much more intense Al(2*p*) peak from Al_2O_3. Similarly, at the low platinum level observed with Pt/molybdena (C), the Pt(4*f*) peaks were partially obscured by the Mo(4*s*) photoline. In both cases the much weaker Pt(4*d*) lines were monitored, with a consequent decrease in signal to noise. Nevertheless, the signals were of sufficient intensity to allow accurate determinations of the Pt(4*d*) binding energies (see Fig. 2). This underscores the ability of state-of-the-art XPS equipment to provide meaningful information on real supported catalysts which typically contain very low metal loadings (*7*).

Inspection of the data in Table 5 reveals the following points. First, the silica- and alumina-supported samples all provide a marked contrast with the two Pt/molybdena series in that the former show very low levels of total surface carbon. The low figures are perhaps particularly surprising for Pt/silica (M) and Pt/alumina (M) which were, throughout the preparative procedure, immersed in toluene. The O : heteroatom ratios in the supports lie within the expected ranges for SiO_2, Al_2O_3, and MoO_3, respectively. The Pt/silica samples

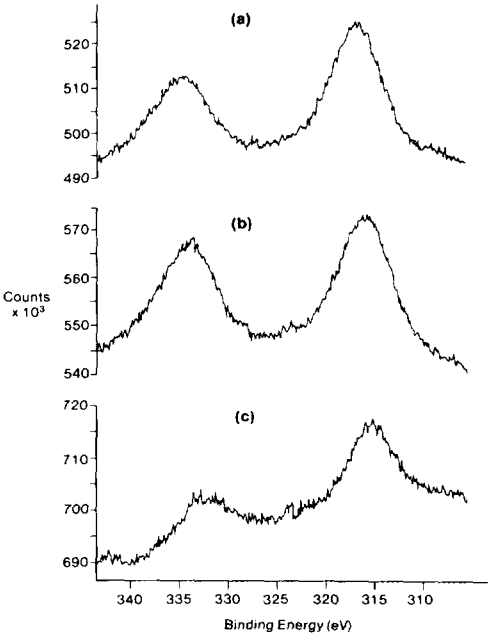

FIG. 2. X-ray photoelectron spectra (unsmoothed) of alumina-supported catalysts. The Pt($4d_{3/2}$, $4d_{5/2}$) doublet for (a) Pt/alumina (I) in the prereduction state, (b) Pt/alumina (I) in the postreduction state, and (c) Pt/alumina (M).

all display very weak platinum signals which are almost on the limits of detection; chloride is also just detectable, but the levels are very low and close comparison between samples is inappropriate. As expected from the microanalytical data (Table 3), significant amounts of surface chloride are detectable on the alumina support. The XPS data closely reflect the additional chloride which is introduced on impregnation of the alumina with aqueous hexachloroplatinic acid. After allowing for the chloride initially present on the alumina support, the surface chloride-to-platinum ratio approximates to 5 : 1, in close agreement with our interpretation of the UV–visible spectroscopic results (which were obtained by diffuse reflectance), but slightly at variance with the ratio of 6 : 1 obtained from microanalysis of the bulk sample. The additional chloride is retained on the surface during, and after, the reduc-

tion process, although it all appears to be associated with the alumina support rather than platinum in the postreduction state (see EXAFS data). The chloride level on Pt/alumina (M) is, as expected, the same as the background level associated with the surface of the alumina support.

The Pt/molybdena samples show relatively "normal" (in the context of XPS) levels of surface carbon, and the XPS results highlight the considerable contrast between the products of the two methods of preparation. In the prereduced state the impregnated catalyst shows significantly higher levels of surface platinum relative to the co-crystallized material even though the bulk platinum analyses (see Table 3) are essentially the same. This presumably reflects the improved sample homogeneity resulting from the co-crystallization method of preparation. For the impregnated catalyst it appears that much of the chloride initially present (Cl/Pt ~ 4/1) is removed from the surface during reduction, which is consistent with the microanalytical data. Also, it may be significant in the context of the molybdenum bronze formation that the surface platinum concentration noticeably decreases during the reduction process. In general the most satisfactory XPS results have been obtained from the impregnated Pt/molybdena samples which give strong Pt and Mo signals (see Fig. 3).

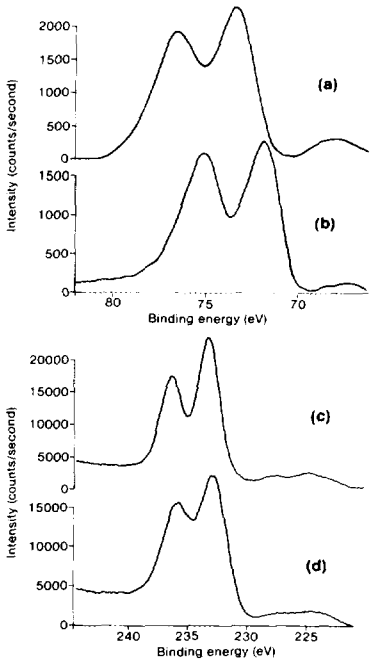

FIG. 3. X-ray photoelectron spectra of molybdena-supported catalysts. The respective Pt($4f_{5/2}$, $4f_{7/2}$) doublets [(a) and (b)] and Mo($3d_{3/2}$, $3d_{5/2}$) doublets [(c) and (d)] for Pt/molybdena (I) in the pre- and postreduction states.

Table 6 summarises the platinum and molybdenum binding energy data for the catalyst samples together with those of various reference materials. Comparison of these data highlights an anomaly. Thus, although electronic spectroscopy and microanalytical data are consistent with the presence of Pt(IV) in the prereduction state, the observed platinum binding energies do in fact compare more favourably with those of the Pt(II) reference compounds. This effect has been noted previously, particularly with Pt/alumina (I) and explanations ranging from surface reduction of platinum (for example, $PtCl_4 \rightarrow PtCl_2$) to charging effects have been advanced (*7, 8*). These may be correct, but the effect may also arise as a simple manifestation of the difference between the XPS experiments on pure compounds and those in which the compounds are highly dispersed on insulating supports.

One point which is clear from the data is that, upon reduction, there is a significant downward shift in Pt binding energy. In the case of Pt/silica (I) the observed values of 315.3 and 71.6 eV for the Pt($4d_{5/2}$) and Pt($4f_{7/2}$) signals are close to that of platinum foil and are thus consistent with the reduction of Pt to the metallic state. Similarly the observed binding energy for Pt/alumina (M) is consistent with the presence of Pt(0), as would be expected from a zero-valent precursor complex. In contrast, the platinum binding energies for Pt/alumina (I) and the Pt/molybdena (I) and (C) samples, in their postreduction states, are significantly higher than the corresponding values of 314.9 and

TABLE 6

Platinum (4*f*), (4*d*) and Molybdenum (3*d*) Binding Energies

Catalyst	Reduction Stage[a]	Binding Energy (eV)			
		Pt($4f_{7/2}$)	Pt($4d_{5/2}$)	Mo($3d_{5/2}$)	
Pt/SiO_2(I)	A	72.7	316.3	—	
	B	71.6	315.3	—	
Pt/SiO_2(M)		72.2	315.8		
Pt/Al_2O_3(I)	A	—	316.6	—	
	B	—	316.1	—	
Pt/Al_2O_3(M)		—	315.3	—	
Pt/MoO_3(I)	A	73.1	316.8	233.3	
	B	71.9	315.5	233.1	230.7
Pt/MoO_3(C)	A	(71.5)	315.2	233.3	
	B	(72.5)	316.0	233.1	230.7
MoO_3		—	—	233.3	
PtO_2		75.6	318.8		
$PtCl_4$		76.1	318.1		
$PtCl_2$		73.4	316.6		
Pt foil		71.4	314.9		

[a] (A) Prereduction; (B) postreduction.

71.4 eV observed with platinum foil. This suggests that in these cases the platinum retains a significant $\delta+$ character after reduction. In Pt/alumina (I) the most likely interpretation is in terms of a metal–support interaction, although this is difficult to confirm on the basis of XPS data alone. Certainly no significant shifts in Al(2*p*) or O(1*s*) binding energies are observed, although unless the effect was very significant these would be obscured by signals from the large excess of "conventional" Al and O in the support material. Nevertheless, supporting evidence for the presence of a metal-support interaction has been obtained from EXAFS data (see later). For the Pt/molybdena samples the suggestion of a platinum $\delta+$ oxidation state after reduction is easier to account for because of the independent evidence for molybdenum bronze formation. This is confirmed by changes noted in the Mo(3*d*) spectra on reduction, whereupon significant broadening of the peaks is observed (see Fig. 3). On deconvolution of the spectra the data can be interpreted in terms of the presence of two oxidation states of molybdenum, namely, Mo(VI) and Mo(IV), without the need to invoke the presence of Mo(V). This is consistent with the formation of the hydrogen bronze. The surface Mo(VI)/Mo(IV) ratios for the impregnated and co-crystallized catalysts are 1.6 and 4, respectively. These correspond to the stoichiometries $H_{0.8}MoO_3$ and $H_{0.4}MoO_3$ and are in good agreement with the TGA and TPR data for the bulk samples.

A final point which requires explanation concerns the apparently anomalous value of the Pt($4d_{5/2}$) binding energy recorded for Pt/molybdena (C) in the prereduction state. The sample examined by XPS was that which had undergone air calcination at 723 K (see TGA data), conditions under which decomposition of platinum oxide to platinum metal is known to occur. The observed binding energy of 315.2 eV therefore represents a true control value for metallic platinum supported on molybdena, against which other values can be compared. The significantly higher binding energy of 316.0 eV observed for Pt/molybdena (C) after "reduction" in H_2/N_2 and bronze formation thus provides conclusive evidence in favour of the $\delta+$ nature of platinum in the bronze.

X-ray diffraction (XRD). One of the platinum/molybdena samples, Pt/molybdena (I), was examined by hot-stage controlled atmosphere XRD in order to ascertain whether a detectable crystalline phase was formed/retained during the simultaneous formation of the molybdenum bronze and reduction of the platinum. The only detectable crystalline phase present prior to heating in 5% H_2/N_2 was MoO_3. On heating the sample changed dramatically at 523 K and at 573 K was totally amorphous over the full $\theta/2\theta$ diffractometer range.

Secondary ion mass spectrometry (SIMS). The three catalysts prepared by aqueous impregnation were examined by SIMS but no evidence of the presence of platinum was obtained. This is attributed to a combination of the known very low sensitivity towards Pt in the SIMS experiment and to the highly dispersed nature of the platinum on the high-surface-area silica and alumina supports. No chloride-con-

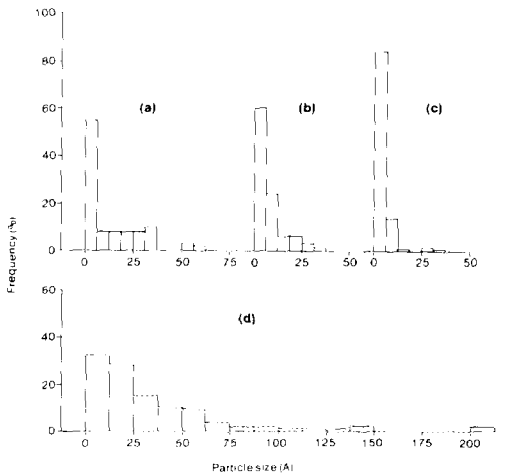

FIG. 4. Particle size distributions as determined by measurement of the electron micrographs of (a) Pt/silica (I), (b) Pt/alumina (I), (c) Pt/molybdena (C), and (d) Pt/molybdena (I).

taining fragments were detected, the only peaks observed being Si–O and Al–O fragments in Pt/silica (I) and Pt/alumina (I), respectively. In the potentially most favourable situation for the detection of platinum, the low-surface-area Pt/molybdena sample, an intense molybdenum spectra was observed, the Mo_2^+ component of which was of sufficiently high intensity to obscure completely the very much weaker signal expected for platinum.

High-resolution transmission electron microscopy (HRTEM). The impregnated and co-crystallized catalysts were examined in their postreduction states by transmission electron microscopy. The electron micrographs which were obtained were of conventional appearance; particle size distributions are shown in Fig. 4. With the exception of Pt/molybdena (I) the catalysts were generally of small particle size, and it is likely that some of the smallest particles escaped detection. Hence the distributions shown in Fig. 4 should only be regarded as a guide to the very high dispersions (approaching 100%) of the active platinum phases in the three catalysts.

Examination of the results shows that the particle size distribution in Pt/alumina (I) is very narrow with most particles less than 40 Å in size and, of these, greater than 60% less than 7 Å. The Pt/SiO_2(I) sample is significantly more heterogeneous in nature with a larger distribution of particle sizes (up to 62 Å) although greater than 55% are still less than 7 Å in size. The evidence, including chemisorption results to be presented in Part II of the series, indicates that the larger particles observed in the TEM contain unresolved aggregates of smaller platinum clusters.

The two molybdena-supported samples provide a very distinct contrast. The particle size distribution within Pt/molybdena (I) is very broad, with large particles of up to 225 Å in size. These large particles have a different morphology from the smaller particles found in this sample, i.e., those less than 100 Å in size, which can be attributed to discrete platinum particles. By contrast the micrographs of Pt/molybdena (C) exhibit few readily observable platinum particles. Careful examination of several micrographs clearly indicates that most (>85%) platinum particles supported on this catalyst are very small, typically 10 Å or less in size. This distribution is narrower than that of any of the samples produced by aqueous impregnation and is presumably another reflection of the method of preparation (although the distinction is at variance with the platinum dispersions measured by CO chemisorptions, see Part II of the series). Thus the average particle sizes in the samples examined by TEM lie in the order Pt/molybdena (C) < Pt/alumina (I) < Pt/silica (I) ≪ Pt/molybdena (I).

Extended X-ray absorption fine structure spectroscopy (EXAFS). EXAFS spectra, the parameters for which are summarised in Table 7, were recorded for three samples, namely, Pt/alumina (I), Pt/alumina (M) and Pt/alumina (I), and Pt/silica (I) in their pre- and postreduction states, respectively. Platinum foil was also measured for comparison purposes and the agreements obtained between experiment and theory are illustrated in Fig. 5.

TABLE 7

EXAFS Parameters

Sample	Shell no.	Atom type	Distance (Å)	Coordination number	Debye–Waller factor
Pt foil	1	Pt	2.77	12.0	0.010
	2	Pt	3.92	6.1	0.014
	3	Pt	4.81	21.9	0.016
	4	Pt	5.47	14.0	0.012
H_2PtCl_6/Al_2O_3(I)	1	Cl	2.31	7.1	0.010
Pt/Al_2O_3(I)	1	Pt	2.72	3.3	0.015
	2	Pt	3.92	0.3	0.004
	3	O	1.94	0.8	0.03
Pt/Al_2O_3(M)	1	Pt	2.71	4.4	0.030
	2	O	2.14	1.9	0.026
	3	Pt	4.77	1.1	0.002
Pt/SiO_2(I)	1	Pt	2.76	4.0	0.011
	2	Pt	3.91	1.5	0.011
	3	Pt	4.78	1.4	0.009
	4	Pt	5.42	2.3	0.010
	5	O	1.93	0.3	0.008

Note. Shells 2, 3, 4, and 5 significant at 1%.

For Pt/alumina (I) the Fourier transform of the material in the prereduction state is dominated by a single peak. The Pt–Cl shell radius of 2.31 Å compares favourably with the expected value of 2.26 Å, and the coordination number (CN) of 7.1 is close to the expected value of 8 in H_2PtCl_6. The absence of Pt–Pt distances confirms that the chloroplatinate (IV) ions are widely dispersed on the support. It will be noted that this interpretation of the EXAFS data is consistent with the Cl/Pt ratios obtained from microanalysis but at variance with the UV–visible spectroscopic data and XPS data which were interpreted in terms of the presence of $[PtCl_5(OH)]^{2-}$ rather than $[PtCl_6]^{2-}$. As far as the EXAFS data are concerned this is equivalent to the replacement of one chloride ion, which is a weak scatterer of X-rays, by an oxide ion, which is an even weaker scatterer. It is quite likely therefore that the sensitivity of the EXAFS results would be insufficient to distinguish between these two possibilities. After reduction the Fourier transform of Pt/alumina (I) is dominated by the single peak of the first platinum shell. The first shell radius is shorter than expected at 2.72 Å, and the coordination numbers for the two platinum shells are much lower than for bulk platinum, suggesting that the average platinum particle is very small. There is also an oxygen shell at 1.94 Å. The experimental values of the coordination numbers show that the average metal particle is best modelled by a five-atom metal cluster in which four are in a first layer in contact with the support with the fifth in a second layer occupying one of the two possible sites. Both the 2^{-2} *r* platinum shell and the oxygen shell are significant when the significance test of Joyner *et al.* is applied (*9*). Additionally, if each of the platinum atoms in the first layer has one oxygen neighbour, then the overall oxygen coordination number will be 0.8, which compares well with the experimental result.

The EXAFS spectrum of Pt/alumina (M) was weak but contained clear structure to 800 eV from the edge. Very good agreement between experiment and theory was obtained (Fig. 5d) for a model involving a first shell of platinum atoms at 2.69 Å with CN = 2.2 (Debye–Waller factor = 0.025), three shells of oxygen atoms at distances from 2.07 to 2.62 Å and CN ~ 1.5, and several further shells of platinum atoms between 3.65 and 5.44 Å having low coordination numbers. Application of the significance test indicated that only three shells were certainly significant and a calculation based on these shells alone gives the information in Table 7. The tabulated data must be understood to mean (i) that most platinum particles are extremely small with an average coordination number in the first shell of 4 ± 1; (ii) the third shell, i.e., the second shell of platinum neighbours, has a low coordination number but the very presence of this shell (standing as it does for the larger number of shells in the more extended calculation) probably indicates the presence of a very small number of larger platinum particles in the sample. The second shell indicates that there are some atoms of low atomic mass about platinum; the calculation represents these as oxygen atoms of the support, but

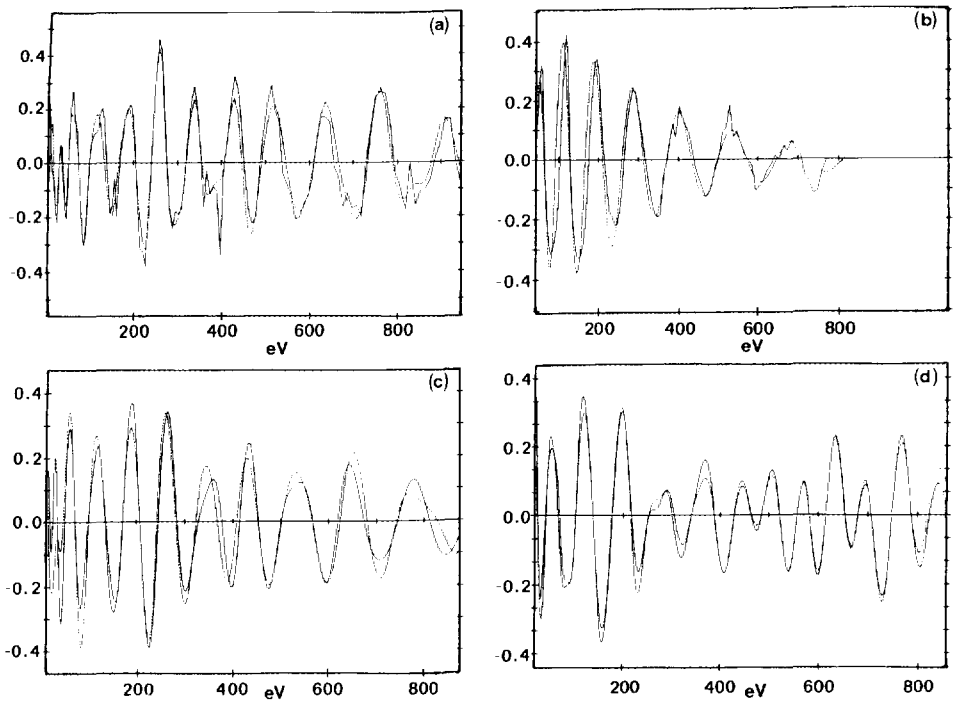

FIG. 5. EXAFS spectra, k^2-weighted of (a) Pt/silica (I) postreduction (unsmoothed spectrum), (b) Pt/alumina (I) prereduction (unsmoothed spectrum), (c) Pt/alumina (I) postreduction (smoothed spectrum), and (d) Pt/alumina (M) in the as-prepared state (smoothed spectrum). In all cases the continuous curve represents the experimental spectrum and the dashed curve the theoretical spectrum calculated using the Daresbury package EXCURV90.

equally these neighbours could be carbon atoms fragments from the ligand toluene, or both.

In the case of Pt/silica (I), reference to Table 7 shows that the shell radii are slightly shorter than for bulk platinum and coordination numbers are significantly lower than those expected for bulk platinum. There is also an oxygen shell at 1.94 Å. Details of the small particle modelling from the EXAFS data for Pt/silica (I) have been described elsewhere (*10*). The most appropriate models are shown in Fig. 6; of these model (c) is preferred. Electron microscopy indicates that the majority (55%) of the platinum particles are in the size range up to 7 Å, although there is a larger distribution of sizes of particles than is the situation for Pt/alumina (I), consistent with the average metal particle model suggested on the basis of the EXAFS data.

Finally, it is significant to note that although chloride was present in the preparations of the catalyst precursors in the case of Pt/alumina (I) and Pt/silica (I), there is no evidence to suggest that chloride is present in detectable amounts in the environment of the platinum in the postreduction state.

The average platinum particle sizes in the

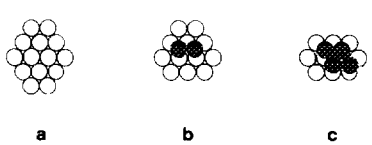

FIG. 6. Proposed model configurations for platinum particles in Pt/silica (I).

TABLE 8

Values of x in the Molybdenum Bronze H_xMoO_3 as Determined by TGA, TPR, and XPS

	TGA	TPR	XPS
$Pt/MoO_3(I)$	0.9	1.2	0.8
$Pt/MoO_3(C)$	0.5	0.4	0.4

samples examined by EXAFS thus lie in the order Pt/alumina (M) < Pt/alumina (I) < Pt/silica (I), in agreement with the data from electron microscopy and CO chemisorption. Perhaps surprisingly, considering the totally different methods of preparation, there is little apparent difference between Pt/alumina (M), as prepared, and Pt/alumina (I) in the postreduction state, although of course considerably less chloride is associated with the former material.

CONCLUSIONS

The six supported platinum catalysts, the preparation and characterisation of which are described in this paper, are, by any comparator, well characterised. We have demonstrated a high degree of internal consistency between (i) results obtained using duplicate techniques at different centres and (ii) results obtained using a variety of different physical techniques. As an example of the latter, the agreement obtained between TGA, TPR, and XPS data for the value of x in H_xMoO_3, the molybdenum bronze component generated during the production of Pt/molybdena (I) and Pt/molybdena (C), is summarised in Table 8.

The preparation and characterisation work has highlighted significant differences between Pt/silica (I) and Pt/alumina (I). Thus, reduced Pt/silica (I) contains platinum in the metallic state and has a chloride content which is no greater than that of the original support, despite its having been prepared from a chloride precursor. This is important, since interpretations in the literature of activity, selectivity, and lifetime characteristics are sometimes confused by the possible effects of residual chloride. We have confirmed that a chloride-free platinum active phase can be prepared from the most commonly used precursor (H_2PtCl_6) by normal methods, carefully and demonstrably controlled. In contrast, Pt/alumina (I) in its postreduction state retains most of the chloride which was present in the initial stages of the catalyst preparation. From chemisorption measurements (see Part II of the series), it appears that the chloride is associated with the support rather than the metal. Evidence from reaction chemistry, in particular the hydrogenation of 1,3-butadiene (see Part IV of the series), also suggests that chloride is not associated with the active platinum site. The platinum itself retains some $\delta+$ character after reduction, which is best attributed to a metal–support interaction.

HRTEM and EXAFS data are self-consistent and, with the exception of Pt/molybdena (I), the platinum crystallites are extremely highly dispersed with size distributions in the order Pt/alumina (M) ~ Pt/silica (M) < Pt/molybdena (C) < Pt/alumina (I) < Pt/silica (I) ≪ Pt/molybdena (I). The platinum entities in Pt/alumina (M) resemble those in Pt/alumina (I), and in each case there is extensive chemical bonding between the platinum ensemble and the support.

These materials provide a unique series of supported platinum catalysts graduated with respect to particle size and extent of metal–support interaction for which detailed chemisorption properties for a range of adsorbates (see Part II of the series) are now known.

ACKNOWLEDGMENTS

We are grateful to SERC and ICI Chemicals and Polymers, Ltd., for their generous financial support of the work described in this paper.

REFERENCES

1. Torrovap Industries, Inc., 90 Nolan Court, Unit 39-40, Markham, Ontario L3R 4L9, Canada.
2. Sing, K. S. W., *in* "Surface Area Determination,

Proc. Int. Symp., Bristol, 1969" (D. H. Everett, Ed.), p. 25. Butterworths, London, 1970.
3. Lever, A. B. P., "Inorganic Electronic Spectroscopy." Elsevier, Amsterdam, 1984.
4. Swihart, D. L., and Mason, W. R., *Inorg. Chem.* **9,** 1749 (1970).
5. Elding, L. I., and Olsson, L. F., *J. Phys. Chem.* **82,** 69 (1978).
6. Dickins, P. G. and Birtill, J. J., *J. Electron. Mater.* **7,** 679 (1978); Greenblatt, M., *Chem. Rev.* **88,** 31 (1988).
7. Barr, T. L., and Yin, M. P., "Characterisation and Catalyst Development," ACS Symposium Series, Vol. 411, p. 203. ACS, Washington, DC, 1989.
8. Bouwman, R., and Biloen, P., *J. Catal.* **48,** 209 (1977).
9. Joyner, R. W., Martin, K. J., and Meehan, P., *J. Phys. C: Solid State Phys.* **20,** 4005 (1987).
10. Jackson, S. D., Keegan, M. B. T., McLellan, G. D., Meheux, P. A., Moyes, R. B., Webb, G., Wells, P. B., Whyman, R., and Willis, J., *in* "Preparation of Catalysts V" (G. Poncelet, P. A. Jacobs, P. Grange, and B. Delmon, Eds.), p. 135. Elsevier, Amsterdam, 1991.